PERGAMON

International Journal of Heat and Mass Transfer 44 (2001) 3953–3961

International Journal of HEAT and MASS TRANSFER

www.elsevier.com/locate/ijhmt

Optimization study and heat transfer comparison of staggered circular and elliptic tubes in forced convection

R.S. Matos [a], J.V.C. Vargas [a,*], T.A. Laursen [b], F.E.M. Saboya [c]

[a] *Departamento de Engenharia Mecânica, Centro Politecnico, Universidade Federal do Paraná, Caixa Postal 19011, Curitiba, PR 81531-990, Brazil*

[b] *Department of Civil and Environmental Engineering, Duke University, Durham, NC, USA*

[c] *Departamento de Engenharia Mecânica, Universidade Federal Fluminense, Niterói, RJ 24210-240, Brazil*

Received 3 August 2000; received in revised form 6 December 2000

Abstract

In this study, a two-dimensional (2-D) heat transfer analysis was performed in circular and elliptic tube heat exchangers. The finite element method was used to discretize the fluid flow and heat transfer governing equations and a 2-D isoparametric, four-noded, linear element was implemented for the finite element analysis program, FEAP (O.C. Zienkiewicz, R.L. Taylor, The Finite Element Method, vol. 1, McGraw-Hill, London, 1989, Chapter 15). The numerical results for the equilateral triangle staggering configuration, obtained with the new element were then validated qualitatively by means of direct comparison to previously published experimental results for circular tubes heat exchangers (G. Stanescu, A.J. Fowler, A. Bejan, Int. J. Heat Mass Transfer 39 (2) (1996) 311–317). Next, a numerical geometric optimization was conducted to maximize the total heat transfer rate between the given volume and the given external flow both for circular and elliptic arrangements, for general staggering configurations. The results are reported for air in the range $300 \leqslant Re_L \leqslant 800$, where L is the swept length of the fixed volume. Circular and elliptical arrangements with the same flow obstruction cross-sectional area were compared on the basis of maximum total heat transfer. The effect of ellipses eccentricity was also investigated. A relative heat transfer gain of up to 13% is observed in the optimal elliptical arrangement, as compared to the optimal circular one. The heat transfer gain, combined with the relative pressure drop reduction of up to 25% observed in previous studies (H. Brauer, Chem. Process Eng., August (1964) 451–460; S.N. Bordalo, F.E.M. Saboya, Determinação experimental dos coeficientes de perda de carga em trocadores de calor de tubos circulares e elípticos aletados, in: Proceedings of the 13th COBEM, Congresso Brasileiro de Engenharia Mecânica (in Portuguese), Belo Horizonte, Brasil, 1995) show that the elliptical arrangement has the potential for a considerably better overall performance than the traditional circular one. © 2001 Published by Elsevier Science Ltd.

1. Introduction

Economic and environmental considerations have brought the need for performance improvement on all engineering applications, aiming to rationalize the use of available energy and reduction of lost work. Many industrial applications require the use of tubes heat exchangers, that have to be sized according to space availability. Therefore, the volume occupied by the array of tubes is fixed. The volume constrained optimization problem consists on finding the optimal spacing between tubes (or cylinders), of a known geometry, such that maximum overall heat transfer (or thermal conductance) between the array and the surrounding fluid is achieved. A typical application of such fundamental optimization results is on the development of cooling techniques for electronic packages. Considerable effort has been put on finding optimal spacings for many different types of geometries, both for natural and forced convection [2,5–15].

Stanescu et al. [2] reported the optimal spacing of circular cylinders in free-stream cross-flow forced

* Corresponding author. Tel.: +55-41-361-3307; fax: +55-41-361-3129.

E-mail address: jvargas@demec.ufpr.br (J.V.C. Vargas).

0017-9310/01/$ - see front matter © 2001 Published by Elsevier Science Ltd.
PII: S0017-9310(01)00006-0

Nomenclature

a	larger ellipse semi-axis, m
A_c	minimum free flow cross-sectional area, m^2
b	smaller ellipse semi-axis, m
c_p	fluid specific heat at constant pressure, J/(kg K)
$C(\tilde{U})$	momentum capacity matrix
D	tube diameter, m
e	ellipses eccentricity, Eq. (20)
F_1, F_2	momentum force vectors
G	energy force vector
$\bar{h}$	equivalent average heat transfer coefficient, W/(m^2 K)
H	array height, m
k	fluid thermal conductivity, W/(m K)
$K_{11}, K_{12}, K_{21}, K_{22}$	viscous stiffness matrices
$\hat{K}_{11}, \hat{K}_{12}, \hat{K}_{21}, \hat{K}_{22}$	penalty matrices
L	array length, m
$\tilde{L}$	diffusive matrix
L/D	array length to diameter aspect ratio
$L/2b$	array length to smaller ellipses axis aspect ratio
$\dot{m}_{ec}$	fluid mass flow rate entering one elemental channel, kg/s
n	normal direction
N	number of tubes in one elemental channel
N_{ec}	number of elemental channels
$\overline{Nu}$	array average Nusselt number
p	pressure, N/m^2
P	dimensionless pressure
Pe_L	Peclet number based on array length
Pr	fluid Prandtl number, ν/α
q	overall heat transfer rate, W
q''_n	local normal heat flux, W/m^2
$\bar{q}''_i$	average normal heat flux at the ith tube surface, W/m^2
$\tilde{q}$	dimensionless overall thermal conductance, Eq. (15)
$\tilde{q}_{max}$	maximum dimensionless overall thermal conductance
$\tilde{q}_*$	dimensionless overall thermal conductance, Eq. (18)
$\tilde{q}_{*,max}$	maximum dimensionless overall thermal conductance
Re_D	Reynolds number based on tube diameter
Re_L	Reynolds number based on array length
S	spacing between rows of tubes, m, Fig. 1
S_{max}	maximum spacing between rows of tubes, m
S/D	dimensionless spacing between rows of tubes (circular arrangement)
$(S/D)_{opt}$	optimal dimensionless spacing between rows of tubes (circular arrangement)
$S/2b$	dimensionless spacing between rows of tubes (elliptic arrangement)
$(S/2b)_{opt}$	optimal dimensionless spacing between rows of tubes (elliptic arrangement)
T	temperature, K
$\bar{T}_{out}$	average fluid temperature at the elemental channel outlet, K
T_w	tube surface temperature, K
T_∞	free stream temperature, K
u, v	velocity components, m/s
U, V	dimensionless velocity components
U_∞	free stream velocity, m/s
W	array width, m
x, y	Cartesian coordinates, m
X, Y	dimensionless cartesian coordinates

Greek symbols

α	thermal diffusivity, m^2/s
γ	penalty factor
ε	mesh convergence criterion, Eq. (19)
θ	dimensionless temperature
$\bar{\theta}_{out}$	dimensionless average fluid temperature at the elemental channel outlet
ν	fluid kinematic viscosity, m^2/s

convection, which followed the study presented by Bejan et al. [13] on the optimization of arrays of circular cylinders in natural convection. Both studies considered only equilateral triangle staggering configurations. The tube geometry was not investigated in those studies as an additional degree of freedom. The elliptic tube geometry is expected to perform better, aerodynamically, than the circular one, i.e., combining reduction in total drag force and increase in total heat transfer, as it was reported by Rocha et al. [16], when comparing elliptic and circular sections in the specific cases of one and two-row tubes and plate fin heat exchangers. The results showed a heat transfer gain of up to 18% when comparing elliptic to circular arrangements in the studied cases.

The present study focuses on the geometric optimization (optimal spacing) of staggered circular and elliptic tubes in a fixed volume. The problem is treated in a fundamental (geometric) sense, without specific reference to an application (electronics cooling, compact heat exchangers, etc). The optimizations are conducted numerically, by using the finite element method to solve the conservation equations (mass, momentum and energy), to obtain the velocity and temperature fields inside the arrays, thereafter computing the overall heat transfer rate between the tubes and the fluid. First, the numerical results obtained with the finite element code are validated by direct comparison to previously published experimental results for circular tubes heat exchangers with equilateral triangle staggering configurations [2]. Next, the equilateral triangle staggering configuration is relaxed and numerical optimization results are obtained for circular and elliptic arrangements, for general staggering configurations. Circular and elliptical arrangements with the same flow obstruction cross-sectional area are then compared on the basis of maximum total heat transfer. Appropriate non-dimensional groups are defined and the optimization results reported in dimensionless charts.

2. Theory

Fig. 1 is a general simple sketch of the problem configuration. It was shown by Fowler and Bejan [17] that in the laminar regime, the flow through a large bank of cylinders can be simulated accurately by calculating the flow through a single channel, such as that illustrated by the unit cell seen in Fig. 1. Because of the geometric symmetries, there is no fluid exchange and no heat transfer between adjacent channels. In Fig. 1, L and H are the length and height of the array, and not shown is the width of the array (tube length), W.

The governing equations are the mass, momentum and energy equations which were simplified in accordance with the assumptions of two-dimensional (2-D) incompressible steady-state flow with constant properties, for a Newtonian fluid:

$$\frac{\partial U}{\partial X}+\frac{\partial V}{\partial Y}=0, \tag{1}$$

$$U\frac{\partial U}{\partial X}+V\frac{\partial U}{\partial Y}=-\frac{\partial P}{\partial X}+\frac{1}{Re_{\mathrm{L}}}\left[\frac{\partial^2 U}{\partial X^2}+\frac{\partial^2 U}{\partial Y^2}\right], \tag{2}$$

$$U\frac{\partial V}{\partial X}+V\frac{\partial V}{\partial Y}=-\frac{\partial P}{\partial Y}+\frac{1}{Re_{\mathrm{L}}}\left[\frac{\partial^2 V}{\partial X^2}+\frac{\partial^2 V}{\partial Y^2}\right], \tag{3}$$

$$U\frac{\partial \theta}{\partial X}+V\frac{\partial \theta}{\partial Y}=\frac{1}{Pe_{\mathrm{L}}}\left[\frac{\partial^2 \theta}{\partial X^2}+\frac{\partial^2 \theta}{\partial Y^2}\right], \tag{4}$$

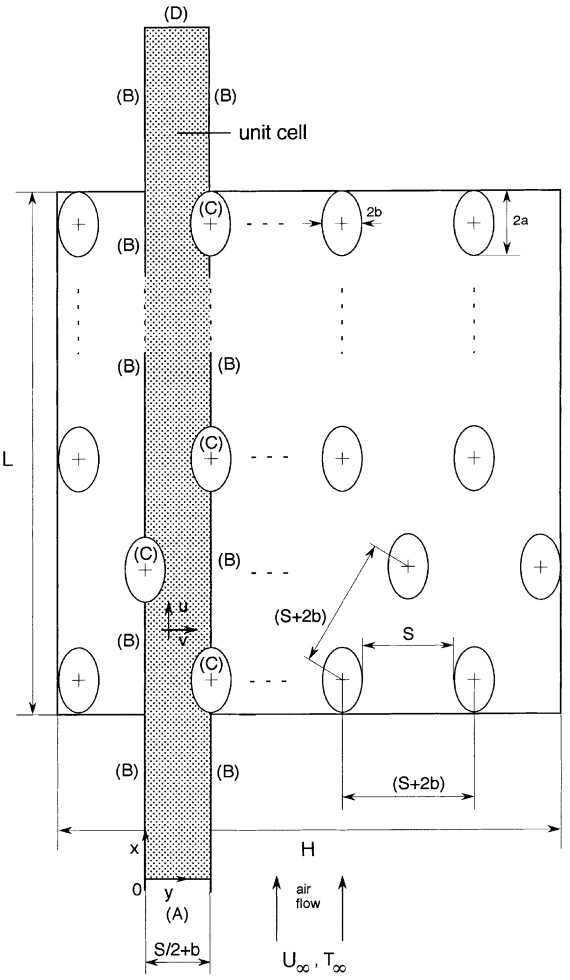

Fig. 1. Problem sketch and computational domain.

where dimensionless variables have been defined as follows:

$$(X,Y)=\frac{(x,y)}{L},\quad P=\frac{p}{\rho U_\infty^2}, \tag{5}$$

$$(U,V)=\frac{(u,v)}{U_\infty},\quad \theta=\frac{T-T_\infty}{T_{\mathrm{w}}-T_\infty},\quad Re_{\mathrm{L}}=\frac{U_\infty L}{\nu},\quad Pe_{\mathrm{L}}=\frac{U_\infty L}{\alpha}, \tag{6}$$

where (x,y) are the Cartesian coordinates, m; p the pressure, N/m^2; ρ the fluid density, kg/m^3; U_∞ the free stream velocity, m/s; (u,v) the fluid velocities, m/s; T the fluid temperature, K; T_∞ the free stream temperature, K; T_{w} the tubes surface temperature, K; L the length of the array in the flow direction, m; ν the fluid kinematic viscosity, m^2/s and α is the fluid thermal diffusivity, m^2/s.

To complete the problem formulation, the following boundary conditions are specified for the extended computational domain of the unit cell of Fig. 1:

$$\text{(A)}\quad U=1,\quad \frac{\partial V}{\partial X}=0,\quad \theta=0, \tag{7}$$

$$\text{(B)}\quad \frac{\partial U}{\partial Y}=0,\quad V=0,\quad \frac{\partial \theta}{\partial Y}=0, \tag{8}$$

$$\text{(C)}\quad U=V=0,\quad \theta=1, \tag{9}$$

$$\text{(D)}\quad \frac{\partial U}{\partial X}=\frac{\partial V}{\partial X}=0,\quad \frac{\partial \theta}{\partial X}=0. \tag{10}$$

Once the geometry of the extended computational domain defined by the unit cell of Fig. 1 is specified, Eqs. (1)–(10) deliver the resulting velocities, pressure and temperature fields in the domain.

The optimization objective is to find the optimal geometry, such that the volumetric heat transfer density is maximized, subject to a volume constraint. The engineering design problem starts by recognizing the finite availability of space, i.e., an available space $L \times H \times W$ as a given volume that is to be filled with a heat exchanger. To maximize the volumetric heat transfer density means that the overall heat transfer rate between the fluid inside the tubes and the fluid outside the tubes will be maximized.

The critical part of an optimization study consists of identifying the degrees of freedom (variables) that allow the maximization (or minimization) of the chosen figure of merit, in this case, the maximization of the overall heat transfer rate between the tubes and the free stream, q. The first variable identified in this way was the spacing between rows of tubes, S. For a given tube arrangement, containing a pre-specified number of elemental channels (or unit cells), N_{ec}, there is a maximum spacing between rows, S_{max}, such that the arrangement fits in the available space, $L \times H \times W$. To justify the choice of the parameter S to be optimized, it is sufficient to analyze two extremes: $S \to 0$ and $S \to S_{max}$. When $S \to 0$, the minimum free flow cross-sectional area, A_c, is reduced, and for a given free stream velocity condition at the arrangement inlet, U_∞, the mass flow rate in the elemental channel is also reduced and, therefore $q \to 0$. When $S \to S_{max}$, A_c increases, thus the flow velocity at the minimum cross-sectional area is reduced, the heat transfer coefficient also decreases and $q \to 0$. This behavior at the extremes clearly indicates the existence of a maximum q in the interval $0 < S < S_{max}$, provided that S_{max} is large enough.

In order to perform the comparison between the elliptic and circular arrangements, a criterion was adopted to preserve similar flow characteristics in the unit cell, i.e., the flow obstruction cross-sectional areas of the arrangements under comparison were made equal. The same criterion was adopted by Rocha et al. [16] for tubes and plate fin heat exchangers. Hence, in all cases, the diameter of the circles, D, was equal to the smaller axis of the ellipses, $2b$.

3. Numerical method

The numerical solution of Eqs. (1)–(10) was obtained utilizing the finite element method [1]. This way, the velocities and temperature fields in the unit cell of Fig. 1 were determined.

The first step in the numerical implementation was the elimination of the pressure variable from Eqs. (2) and (3), by using a penalty model, approximating Eq. (1) as follows [18]:

$$\frac{\partial U}{\partial X}+\frac{\partial V}{\partial Y}=-\frac{P}{\gamma}, \tag{11}$$

where γ is the penalty factor, which must be assumed large enough in order to satisfy mass conservation approximately.

The implementation of the finite element method for the solution of Eqs. (1)–(10) starts from obtaining the variational (weak) form of the problem. Next, the weak form is discretized, by a suitable method. Due to the characteristics of the flow inside the arrangement of Fig. 1, physically, it is seen that the solution at a specified location in the unit cell depends preferably on what happens upstream, considering the direction of the forced flow. It is well known that the Galerkin method, which is the analogue of a central differences scheme in the finite differences method, does not capture this physical aspect in its discretized equations. Therefore, the discretization utilized in this work is an 'upwind' scheme proposed by Hughes [19], where it is possible to adequate the discrete form of the problem to the physical characteristics of the flow.

After developing the discrete form of the problem, the resulting algebraic equations are arranged in a matricial form for the steady-state 2-D problem as follows:

$$\begin{bmatrix} C(\tilde{U}) & 0 \\ 0 & C(\tilde{U}) \end{bmatrix} \begin{Bmatrix} \tilde{U}_1 \\ \tilde{U}_2 \end{Bmatrix} + \begin{bmatrix} 2K_{11}+K_{22} & K_{21} \\ K_{12} & K_{11}+2K_{22} \end{bmatrix} \begin{Bmatrix} \tilde{U}_1 \\ \tilde{U}_2 \end{Bmatrix} + \begin{bmatrix} \hat{K}_{11} & \hat{K}_{12} \\ \hat{K}_{21} & \hat{K}_{22} \end{bmatrix} \begin{Bmatrix} \tilde{U}_1 \\ \tilde{U}_2 \end{Bmatrix} = \begin{Bmatrix} F_1 \\ F_2 \end{Bmatrix}, \tag{12}$$

$$\tilde{D}(\tilde{U})\tilde{T}+\tilde{L}\tilde{T}=G, \tag{13}$$

where $C(\tilde{U})$ is the capacity matrix that contains the advective terms of the momentum equations, which

depends non-linearly on the solution $\tilde{U}$ (bipartitioned vector: $\tilde{U}_1$ – direction X and $\tilde{U}_2$ – direction Y, each one with a number of components equal to the number of unknowns in the mesh); K_{11}, K_{12}, K_{21} and K_{22} are the stiffness matrices with constant coefficients (constant viscosity), that contain the viscous terms of the momentum equations; $\hat{K}_{11}, \hat{K}_{12}, \hat{K}_{21}$ and $\hat{K}_{22}$ are the penalty matrices, that contain the terms due to the elimination of the pressure variable from the momentum equations by using Eq. (11), which were computed with reduced integration (one point in each direction with linear shape functions) to avoid locking; $\tilde{D}(\tilde{U})$ is the capacity matrix that contain the advective terms of the energy equation; $\tilde{L}$ is the diffusive matrix with constant coefficients (constant thermal conductivity), that contain the diffusive terms from the energy equation; F_1 and F_2 are the force vectors of the momentum equations that contain the field forces and the velocity boundary conditions, and G is the force vector of the energy equation that contains the heat source terms of the energy equation and the temperature boundary conditions.

For the sake of brevity, the mathematical details of the components of the above-described matrices are not presented. However, the reader is directed to the work of Reddy and Gartling [20], which was the basis for the formulation implemented computationally in the present study. A Fortran subroutine was written to implement the Navier–Stokes and Energy equations in two dimensions as an isoparametric, four-noded, linear element, which was then aggregated to the open code called 'finite element analysis program', FEAP, originally written by Zienkiewicz and Taylor [1].

4. Results and discussion

The non-linear system built from Eqs. (12) and (13) was solved by the Newton–Raphson method [20], to obtain the velocities and temperatures in the computational domain of Fig. 1.

The dimensionless overall thermal conductance $\tilde{q}$, or volumetric heat transfer density for the circular arrangements was defined as follows, for the sake of comparison with the results of Stanescu et al. [2]:

$$\tilde{q} = \frac{q/(T_w - T_\infty)}{kLHW/(2b)^2}, \tag{14}$$

where the overall heat transfer rate between the tubes and the free stream, q, has been divided by the constrained volume, LHW; k is the fluid thermal conductivity, W/(m K), and $2b = D$ the ellipse smaller axis or tube diameter.

The calculation of $\tilde{q}$ is conducted numerically, for the circular configuration, re-arranging Eq. (14) as follows:

$$\tilde{q} = \frac{N_{ec}}{2}\left[\frac{D}{L}\right]^2 \frac{D}{H}\sum_{i=1}^{N}\left[\frac{\bar{q}_i'' L\pi}{k(T_w - T_\infty)}\right], \tag{15}$$

where $\bar{q}_i''$ is the average normal heat flux at the ith tube surface, W/m^2; N is the number of tubes in one elemental channel.

In Eq. (15), $\bar{q}_i''$ is calculated from the local normal heat flux at the tube surface given by

$$q_i'' = k\left(\frac{\partial T}{\partial n}\right)_i, \quad i = 1, \ldots, N, \tag{16}$$

where n denotes the normal direction.

The computation of the heat fluxes for Eq. (16) is done by post-processing the temperature results obtained from the finite element solution.

For the comparison between the elliptic and circular arrangements, the dimensionless overall thermal conductance is computed alternatively from a balance of energy in one elemental channel, noting that:

$$q = N_{ec}\dot{m}_{ec}c_p(\bar{T}_{out} - T_\infty), \tag{17}$$

where $\dot{m}_{ec} = \rho U_\infty((S + 2b)/2)W$, which is the fluid mass flow rate entering one elemental channel, kg/s; c_p is the fluid specific heat at constant pressure, J/(kg K), and $\bar{T}_{out}$ is the average fluid temperature at the elemental channel outlet.

The dimensionless overall thermal conductance computed by Eq. (14), using Eq. (17) is therefore renamed as $\tilde{q}_*$. The calculation of $\tilde{q}_*$ is conducted numerically, re-arranging Eq. (14) as follows:

$$\tilde{q}_* = \frac{N_{ec}}{2} PrRe_L\left[\frac{2b}{L}\right]^2 \frac{2b}{H}\left(\frac{S}{2b} + 1\right)\bar{\theta}_{out}, \tag{18}$$

where Pr is the fluid Prandtl number, ν/α.

The results obtained from Eq. (18) are therefore expected to be more accurate than the results obtained with Eq. (15). The reason is that the former are obtained directly from the finite element temperature solution, whereas the latter are obtained from post-processing the finite element solution. It is well known that the numerical error in the derivative of the solution is larger than the numerical error in the solution itself.

To obtain accurate numerical results, several mesh-refinement tests were conducted. The monitored quantity was the dimensionless overall thermal conductance, computed either with Eq. (15) or with Eq. (18), according to the following criterion:

$$\varepsilon = \left|\tilde{q}_{*,j} - \tilde{q}_{*,j-1}\right| \Big/ \left|\tilde{q}_{*,j}\right| \leqslant 0.01, \tag{19}$$

where j is the mesh iteration index, i.e., as j increases the mesh is more refined. When the criterion is satisfied, the $j - 1$ mesh is selected as the converged mesh.

The criterion defined by Eq. (19) was used to test the extension of the computational domain defined in the

unit cell of Fig. 1. An extra-length $L/2$ had to be added to the computational domain, upstream and downstream of the unit cell to represent the actual flow, and satisfied Eq. (19), when compared to an extra-length L. The last three mesh iterations had (a) 2730 nodes and 2508 elements; (b) 5460 nodes and 5180 elements, and (c) 5670 nodes and 5380 elements, with a relative error below 3%, comparing (a) and (b), and below 1%, comparing (b) and (c), according to Eq. (19). Therefore, for all cases the mesh was established with 5460 nodes and 5180 elements. All meshes were more refined in the regions close to the tubes where the highest gradients in the solution were expected.

The numerical results obtained with the finite element code are validated by direct comparison to previously published experimental results for circular tubes heat exchangers with equilateral triangle staggering configurations obtained with $L = 39.2$ mm, $H = 35.2$ mm, $W = 134$ mm and $D = 6.35$ mm [2].

All the arrangements in this study (elliptic and circular) had $N_{ec} = 6$ and $N = 4$.

The numerical results shown in Fig. 2 were obtained with Eq. (15). Fig. 2 also shows the experimental results obtained by Stanescu et al. [2] for $Re_D = U_\infty D/\nu = 50$ and 100. The experimentally determined $\tilde{q}$ agrees qualitatively with the numerical results, mainly with respect to the identification of $(S/D)_{opt}$. The agreement is remarkable, mainly with respect to the identification of the optimal spacings, if we think that the tested array was not a large bank of cylinders and, in the experiments, with uniform heat flux, while in the numerical simulations it was infinitely wider (i.e., no influence from the wind tunnel walls) and with isothermal cylinders.

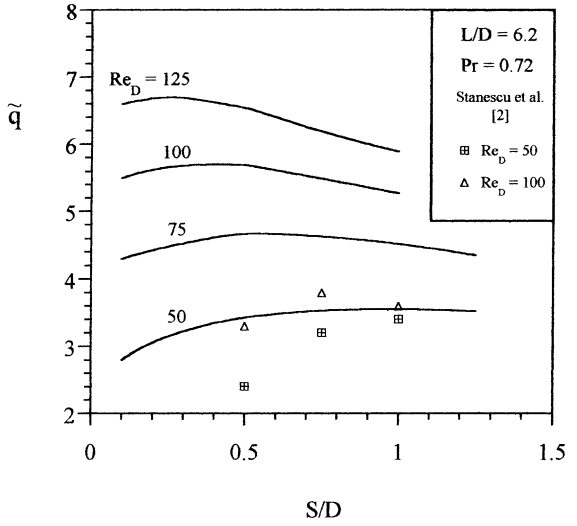

Fig. 2. Numerical and experimental results for circular tubes heat exchangers with equilateral triangle staggering configurations.

Next, numerical optimization results (i.e., identification of the maxima) are obtained for the circular and elliptic arrangements, for general staggering configurations. The dimensionless thermal conductance is hereafter computed with Eq. (18), in the form of $\tilde{q}_*$.

Figs. 3–5 show maxima for $\tilde{q}_*$ with respect to $(S/2b)$, for three different values of ellipses eccentricity, i.e., $e = 1$ (circle), 0.8 and 0.65:

$$e = \frac{b}{a}, \tag{20}$$

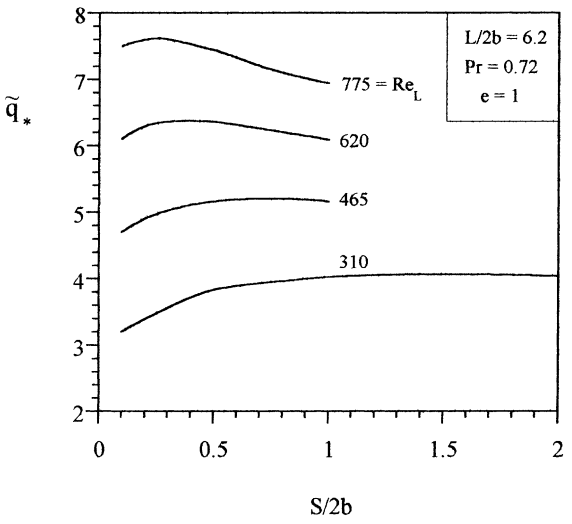

Fig. 3. Numerical results for circular tubes ($e = 1$) heat exchangers with general staggering configurations.

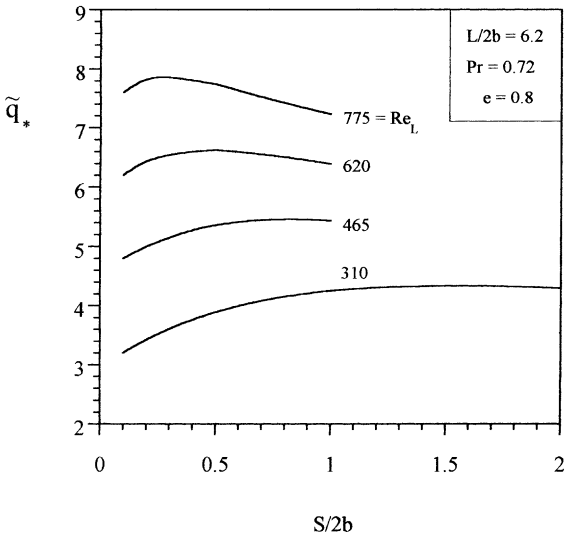

Fig. 4. Numerical results for elliptic tubes ($e = 0.8$) heat exchangers with general staggering configurations.

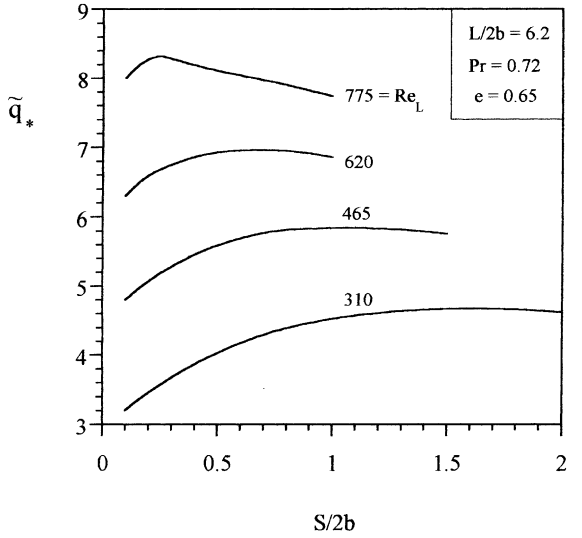

Fig. 5. Numerical results for circular tubes ($e = 0.65$) heat exchangers with general staggering configurations.

where b is the smaller ellipse semi-axis and a is the larger ellipse semi-axis.

The influence of the variation of Re_L is also investigated in Figs. 3–5. As Re_L increases $\tilde{q}_*$ increases. The maximum is less pronounced for lower values of Re_L.

Figs. 6 and 7 show the effect of ellipses eccentricity on $\tilde{q}_*$, for $Re_L = 465$ and 620, respectively. As the eccentricity decreases, $\tilde{q}_*$ increases, therefore the elliptic geometry improves the overall heat transfer rate between the tubes and the free stream.

The results reported in Figs. 4–7 are summarized in Figs. 8 and 9. The effect of ellipses eccentricity on $\tilde{q}_{*,\max}$ is depicted in Fig. 8, where, for all Re_L, $\tilde{q}_{*,\max}$ increases as the eccentricity decreases, i.e., the flatter the ellipses are the higher the overall heat transfer will be. In a quantitative analysis, it is important to stress that a 13% maximum relative heat transfer gain, in comparison with the traditional circular arrangement, was observed for the elliptical arrangement with $e = 0.65$, in the numerical simulations. Fig. 9 shows that the optimal spacing decreases as the free stream velocity (or Re_L) increases.

There was no loss of generality of the optimization results by fixing $N_{ec} = 6$ in the present study, as it is deduced through Eqs. (15) and (18), dividing both sides by N_{ec}. The effect of varying the number of tubes in one elemental channel, N, is still to be investigated, but it should be noted that $N = L/a$ represents the limit where

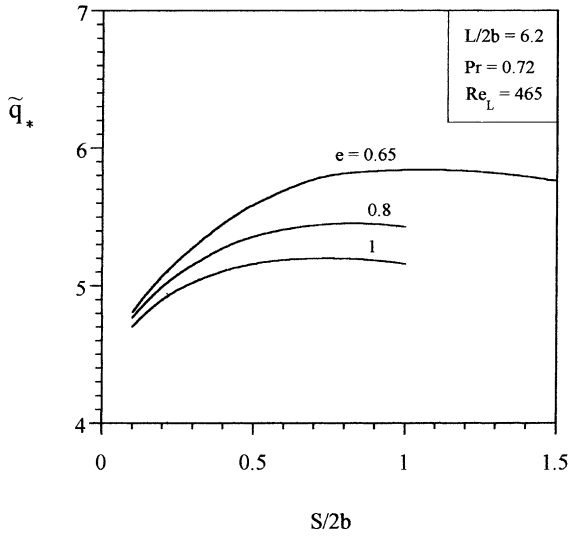

Fig. 6. The effect of ellipses eccentricity on $\tilde{q}_*$ ($Re_L = 465$).

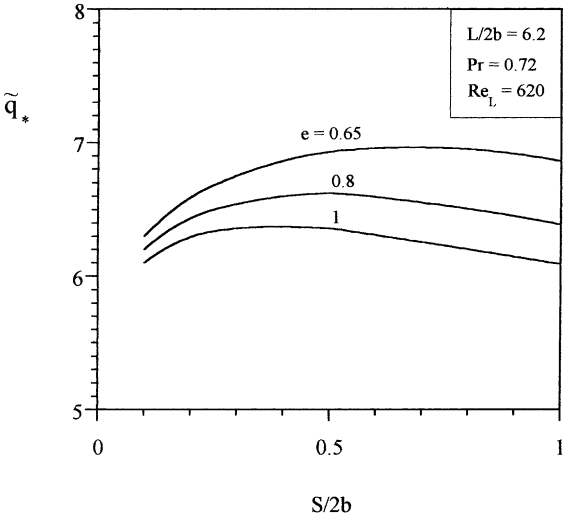

Fig. 7. The effect of ellipses eccentricity on $\tilde{q}_*$ ($Re_L = 620$).

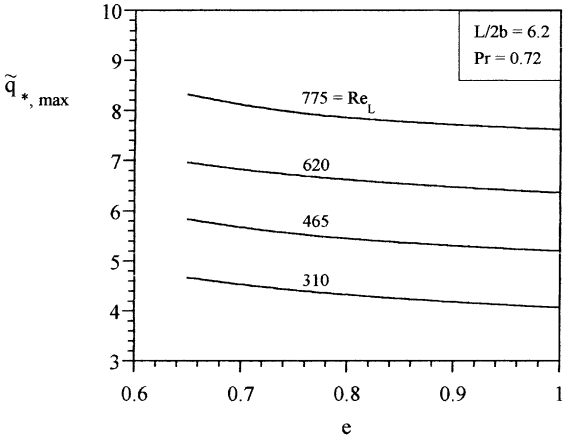

Fig. 8. The effect of ellipses eccentricity on the maximum overall thermal conductance.

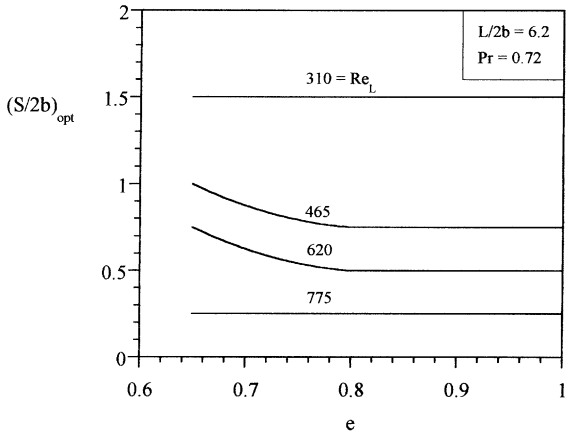

Fig. 9. The effect of ellipses eccentricity on the optimal spacing for maximum overall thermal conductance.

the ellipses ends (edges) touch. However, it is not difficult to verify that the figure of merit given by Eq. (14) is an analogue of the average Nusselt number for the whole arrangement, $\tilde{q} = \overline{Nu} = \bar{h}(2b)/k$, noting that $\bar{h} = q(2b)/((T_w - T_\infty)LHW)$, where $\bar{h}$ is the equivalent average heat transfer coefficient, W/(m^2 K). Therefore, for a larger number of rows, $\tilde{q}_{max}$ (or $\tilde{q}_{*,max}$) computed for $N = 4$ is a fairly good approximation. This is explained by the fact that, with a large number of rows, the flow will be fully developed, therefore with no significant changes in the average Nusselt number for a particular geometry, either circular or elliptic. This behavior was observed experimentally comparing three-row circular results reported by Saboya and Sparrow [21], with two-row circular results reported by Rosman et al. [22], both for finned heat exchangers. The same phenomenon was also observed numerically in a recent study by Fowler et al. [15], for staggered plates in forced convection, where it was reported that the effect of N on $\tilde{q}_{max}$ is almost non-existent for $2 \leqslant N \leqslant 65$.

5. Conclusions

This study demonstrates that the geometric arrangement of staggered circular or elliptic tubes can be optimized for maximum heat transfer (or maximum thermal conductance), when the optimization is subjected to an overall volume constraint. The existence of optimal spacings between rows of tubes was demonstrated through numerical results obtained from two alternative ways, i.e., Eqs. (15) and (18). The approach was to formulate the problem fundamentally as a volume-constrained geometric optimization study, where appropriate non-dimensional groups were identified and generalized results presented in dimensionless charts. From the point of view of practical application of the results herein presented, it is important to stress that they will apply depending on how similar the actual design under consideration is to the configuration presented in Fig. 1, such that the approximate optimal geometry can be predicted. However, from the fundamental point of view, the results show that there will always be an optimal spacing between rows of tubes in circular and elliptic tubes heat exchangers, which is important to be found.

From the heat transfer point of view, it was shown that the elliptic configuration performs better than the circular one. Among the studied cases, a maximum relative heat transfer gain was of 13%, for $e = 0.65$, with $Re_L = 465$. The heat transfer gain, combined with the relative pressure drop reduction of up to 25% observed in previous studies [3,4] show the elliptical arrangement has the potential for a considerably better overall performance than the traditional circular one.

Acknowledgements

The authors acknowledge with gratitude the support of the Program of Human Resources for the Oil Sector and Natural Gas, of the Brazilian Oil National Agency PRH – ANP/MME/MCT.

References

[1] O.C. Zienkiewicz, R.L. Taylor, The Finite Element Method, vol. 1, McGraw-Hill, London, 1989 (Chapter 15).
[2] G. Stanescu, A.J. Fowler, A. Bejan, The optimal spacing of cylinders in free-stream cross-flow forced convection, Int. J. Heat Mass Transfer 39 (2) (1996) 311–317.
[3] H. Brauer, Compact heat exchangers, Chem. Process Eng. August (1964) 451–460.
[4] S.N. Bordalo, F.E.M. Saboya, Determinação experimental dos coeficientes de perda de carga em trocadores de calor de tubos circulares e elípticos aletados, in: Proceedings of the 13th COBEM, Congresso Brasileiro de Engenharia Mecânica, Belo Horizonte, Brasil, 1995 (in Portuguese).
[5] A. Bar-Cohen, W.M. Rohsenow, Thermally optimum spacing of vertical, natural convection cooled, parallel plates, J. Heat Transfer 106 (1984) 116–123.
[6] S.H. Kim, N.K. Anand, L.S. Fletcher, Free convection between series of vertical parallel plates with embedded line heat sources, J. Heat Transfer 113 (1991) 108–115.
[7] R.W. Knight, J.S. Goodling, D.J. Hall, Optimal thermal design of forced convection heat sinks – analytical, J. Electron. Packaging 113 (1991) 313–321.
[8] N.K. Anand, S.H. Kim, L.S. Fletcher, The effect of plate spacing on free convection between heated parallel plates, J. Heat Transfer 114 (1992) 515–518.
[9] R.W. Knight, J.S. Goodling, B.E. Gross, Optimal thermal design of air cooled forced convection finned heat sinks – experimental verification, IEEE Trans. Comp. Hybrids Manufact. Technol. 15 (1992) 754–760.

[10] A. Bejan, E. Sciubba, The optimal spacing of parallel plates cooled by forced convection, Int. J. Heat Mass Transfer 35 (1992) 3259–3264.
[11] A. Bejan, A.M. Morega, Optimal arrays of pin fins in laminar forced convection, J. Heat Transfer 115 (1993) 75–81.
[12] A. Bejan, Convection Heat Transfer, 2nd edition, Wiley, New York, 1995 (Chapters 2–3).
[13] A. Bejan, A.J. Fowler, G. Stanescu, The optimal spacing between horizontal cylinders in a fixed volume cooled by natural convection, Int. J. Heat Mass Transfer 38 (11) (1995) 2047–2055.
[14] G.A. Ledezma, A.M. Morega, A. Bejan, Optimal spacing between fins with impinging flow, J. Heat Transfer 118 (1996) 570–577.
[15] A.J. Fowler, G.A. Ledezma, A. Bejan, Optimal geometric arrangement of staggered plates in forced convection, Int. J. Heat Mass Transfer 40 (8) (1997) 1795–1805.
[16] L.A.O. Rocha, F.E.M. Saboya, J.V.C. Vargas, A comparative study of elliptical and circular sections in one and two-row tubes and plate fin heat exchangers, Int. J. Heat Fluid Flow 18 (1997) 247–252.
[17] A.J. Fowler, A. Bejan, Forced convection in banks of inclined cylinders at low Reynolds numbers, Int. J. Heat Fluid Flow 15 (1994) 90–99.
[18] T.J.R. Hughes, W.K. Liu, A. Brooks, Review finite element analysis of incompressible viscous flows by penalty function formulation, J. Comput. Phys. 30 (1979) 1–60.
[19] T.J.R. Hughes, A simple scheme for developing upwind finite elements, Int. J. Numer. Meth. Eng. 12 (1978) 1359–1365.
[20] J.N. Reddy, D.K. Gartling, The Finite Element Method in Heat Transfer and Fluid Dynamics, CRC Press, Boca Raton, FL, 1994 (Chapters 4–5).
[21] F.E.M. Saboya, E.M. Sparrow, Experiments on a three-row fin and tube heat exchangers, J. Heat Transfer 98 (1976) 520–522.
[22] E.C. Rosman, P. Carajilescov, F.E.M. Saboya, Performance of tube of one and two-row tube and plate fin heat exchangers, J. Heat Transfer 106 (1984) 627–632.